Applied Mathematics & Information Sciences
An International Journal

http://dx.doi.org/10.12785/amis/090633

Fusion of Completed Local Binary Pattern Features with Curvelet Features for Mammogram Classification

Syed Jamal Safdar Gardezi[1,2,*] *and Ibrahima Faye*[1,2,*]

[1] Center for Intelligent Signals and Imaging Research (CISIR), Universiti Teknologi PETRONAS, 32610 Bandar Seri Iskandar, Perak Darul Ridzuan, Malaysia
[2] Department of Fundamental and Applied Sciences, Universiti Teknologi PETRONAS, 32610 Bandar Seri Iskandar, Perak Darul Ridzuan, Malaysia

Received: 6 Nov. 2014, Revised: 28 Jan. 2015, Accepted: 12 Feb. 2015
Published online: 1 Nov. 2015

Abstract: In this paper, fusion of texture features to improve classification accuracy by false positive reduction in mammograms is proposed. The method uses texture features obtained from completed local binary pattern (CLBP) and grey level texture features obtained from the Curvelet sub-bands. In the current experiments, mass and normal patches were obtained from Mammographic image analysis Society (MIAS) and Image retrieval in medical applications (IRMA) datasets for mammograms. Texture features from both methods are combined together to obtain the feature fusion matrix. Then Nearest neighbor classifier was used for classification to evaluate the individual as well as enhanced features obtained from CLBP and curvelet. The classifier produces a classification accuracy of 96.68% with 98.9% sensitivity and the false positive (FP) rates drop by 40% and 78% respectively for the enhanced features as compared to the original results produced by both methods. The experimental results suggest that fusion of features improves the performance of the system and is statistically significant.

Keywords: False positive reduction, Classification, Mammograms, Texture features, Curvelet.

1 Introduction

Women are most affected by breast cancer around the world. According to the International Agency for Research on Cancer (IARC) for the World Health Organization (WHO)reports that more than 522,000 fall victim to breast cancer in 2012 only , and the statistics show an increase of 20% in the breast cancer incidences since 2008 .While the mortality rates increased up to 14%. Moreover, 1.7 million (11.9%) women around the world have chances to suffer from breast cancer during their life time [1]. Early detection is the key to reduce the mortality rates. Texture analysis of an image plays an important role in object recognition, and is an active topic of research in computer vision and pattern recognition. Image texture analysis has been successfully used in areas like biomedical image analysis, face image analysis, video retrieval environment and remote sensing of data for pattern recognition [2].

Many studies have been presented that use the texture information for mammogram classification. Faye et al. [3] proposed a wavelet and curvelet based feature extraction model on mammograms. The significant features were selected using t-test, and support vector machine (SVM) was used for classification. Christoyianni et al. [4] used neural network for classification of suspicious regions in mammograms. The texture features were extracted from the region of interest (ROI). Significant features were selected using the independent component analysis to train the neural network. Karahaliou et al. [5] presented a method for the texture analysis of micro-calcifications in mammograms using wavelet decomposition. Four types of texture features that include first order statistics, co-occurrence matrices features, run length matrices features and Laws' texture energy measures were computed. K-nearest neighbor (kNN) classifier was used to classify benign and malignant classes using the feature matrix. In a similar type of study Gardezi et al. [6] used texture features obtained from the curvelet sub-bands for classification of normal and abnormal mammograms. They constructed grey level co-occurrence matrices from the curvelet sub-bands coefficients and used simple

* Corresponding author e-mail: jamalgardezi@gmail.com, ibrahima_faye@petronas.com.my

logistic classifier for classification. Oliver et al. [7] used local binary pattern (LBP) and co-occurrence matrices to extract texture features from the mammogram ROIs. They employed leave one out (LOO) strategy together with support vector machine (SVM) to obtain the best classification rate. In a similar study, Oliver et al. [8] used LBP texture features for false positive reduction in mammograms. Paquerault et al. [9] fused textural features and morphological features obtained from the region of interest(ROI) to improve the detection of normal and abnormal tissues in mammogram images. Their study revealed an improvement in classification accuracy as well as reduction on false positive (FP) rate. Duarte et al. [10] evaluated the performance of completed local binary pattern (CLBP) and wavelet transform for feature extraction and classification of mammogram lesions. Eltoukhy et al. [11] classified benign and malignant tumors in mammograms on basis of texture analysis of the curvelet features. The most significant texture features were selected from the region of interest, based on Euclidian distance, and classified using the nearest neighbor classifier. Choi et al. [12] presented a method for false positive reduction using multiresolution LBP features, capable to distinguishing between the normal texture patterns and the mass texture regions. Hussain [13] proposed a method to reduce false positives. His method used weber law descriptor (WLD) to extract the local histogram information and integrated it with the spatial information obtained from WLD extension Multiscale spatial weber law descriptor (MSWLD) for the characterization of texture micro structures of masses in mammograms and achieved good results.

The current work aims to improve the classification rate not only in terms of accuracy but also in terms of sensitivity and specificity. The texture features are obtained by completed local binary pattern (CLBP) and curvelet sub-bands texture features. Performance for each method is evaluated separately and later fusion of feature matrices is done to obtain the best classification rate. The study also analyzes the effects of fusion on false positive (FP), whether the fusion of features reduces the FP alarms compared to the individual FP produced by each method or not. The rest of the paper is organized as follows: Section (2) presents a brief overview of Completed Local Binary Pattern (CLBP), and Curvelet transform. Section (3) deals with Experimental details which include dataset, feature extraction and classification details. To measure statistical significance of the method the t-test is discussed in statistical analysis, Section (4). The experimental results and their significance is presented in the Results and discussion section (5) of this paper. The conclusion of the current study is presented in Section (6).

2 Completed Local Binary Pattern (CLBP)

2.1 A brief overview of LBP

Several studies based on the extraction of local patterns (texture analysis) has been developed and tested for mammogram classification [14,15,11,6]. One such method was introduced by Ojala et al. [16] to explore the rotational invariant texture features. The essential idea is based on the signed contrast of local region created for parameters R, P where R denotes the radius of the circular region and P the partition points in its circumference. The extracted patterns are binarized and a histogram measure is computed to synthesize the image information. Ojala et al. [16] termed these outcome from the image as local binary patterns (LBP).

Mathematically, given any pixel in an image, Ojala et al. [16] computed LBP by comparison with its neighboring pixels by the formula given as

$$LBP_{P,R} = \sum_{p=0}^{P-1} s(g_p - g_c)2^P, s(x) = \begin{Bmatrix} 1 & ,x \geq 0 \\ 0 & ,x < 0 \end{Bmatrix} \quad (1)$$

where g_c represent the gray level value of the central pixel under study, g_p is gray value of neighboring pixel, P is the number of neighboring pixels involved and R is the radius of the neighborhood. LBP commonly uses two different transitions to compute the textural features namely uniform LBP and the rotationally invariant uniform patterns .The uniform patterns are represented as $LBP^{u2}_{P,R}$ where "u2" stands for uniform pattern with value of $U \leq 2$ and produces $P*(P-1)+3$ distinct outputs.

$$LBP^{u2}_{P,R} = |s(g_{P-1} - g_c) - s(g_0 - g_c)| + \sum_{p=1}^{P-1} \left|s(g_p - g_c) - s(g_{p-1} - g_c)\right| \quad (2)$$

While the rotationally invariant uniform pattern are denoted as $LBP^{riu2}_{P,R}$, where the "riu2" stands for rotationally invariant uniform with value of $U \leq 2$ and produces $P+2$ distinct output values.

$$LBP^{riu2}_{P,R} = \begin{Bmatrix} \sum_{p=0}^{P-1} s(g_p - g_c)2^P & U(LBP_{P,R}) \leq 2 \\ P+1 & otherwise \end{Bmatrix} \quad (3)$$

Currently there are many extensions of the basic LBP technique that also include information from local absolute value of the contrast, pixel intensities and even local gradients.

2.2 Completed Local binary pattern (CLBP)

Guo et al. [17] presented an extension to LBP called as completed local binary pattern (CLBP), defined by the

regional local central pixel and local difference of sign-magnitude transform (LDSMT). The central pixel is defined by a binary global thresholding map named as CLBP_Centre or CLBP_C while the LDSMT constitutes of two components, namely: difference of signs and difference of magnitudes denoted as CLBP_S and CLBP_M respectively. CLBP_C, CLBP_S and CLBP_M (Figure. 1) are combined to form final CLBP histograms. The LDSMT is mathematically expressed as given central pixel and gray level of neighboring pixel the local difference is defined as $d_p = (g_p - g_c)$,where local difference has two further components sign s_p and magnitude m_p defined as

$$d_p = s_p \times m_p \qquad and \qquad \left\{ \begin{matrix} s_p = sign(d_p) \\ m_p = |d_p| \end{matrix} \right\} \quad (4)$$

The CLBP achieves a better rotational invariant as compared to LBP. However one should note that CLBP_S is same as conventional LBP. The CLBP_S i.e. (LBP) preserves local structural information better than its counterpart CLBP_M.
CLBP_M is defined as

$$CLBP\_M_{P,R} = \sum_{p=0}^{P-1} t(m_p, c)2^p, t(x,c) = \left\{ \begin{matrix} 1, x \geq c \\ 0, x < c \end{matrix} \right\} \quad (5)$$

where c is the adaptive thresholding
Similarly CLBP_C is computed as

$$CLBP\_C_{P,R} = t(g_c, C_I) \quad (6)$$

where t is defined in (5) and C_I are the mean of gray values of the whole images. Like the conventional LBP the CBLP also has two transitions i.e. $CLBP^{u2}_{P,R}$ and $CLBP^{riu2}_{P,R}$. Guo et al. [17] further presented variants of CLBP by concatenating the above defined mappings and defined (CLBP_S/M) that combine sign and magnitude values (S represents the sign), (CLBP_M/C) that combines magnitude and intensities (where C stands for pixel intensity at region Center), (CLBP_S/M/C) combining the three measures and (CLBP_S_M/C) obtained by concatenation of joint histogram operations of sign, magnitude and center pixel intensities.

2.3 Curvelet transform

Often images/signals exhibit discontinuous behavior along curves/peaks also called as curve singularities. In medical images one of the primary tasks is to extract image features. These features could be points, line edges or some texture descriptions. Multiresolution techniques like wavelet and ridgelet have failed to exploit the full potential of these directional/geometric shape features.

To overcome these deficiencies curvelet transform was introduced by Candes and Donoho [18]. The curvelet provided a good reconstruction of images and sparse representation of edges [19]. Curvelet has superior direction representation due to its construction than its predecessor. It obeys the curvelet scaling law i.e. $width \sim length^2$.

In a two dimensional space, with spatial domain x and frequency variable, ω having radius, r and angle θ in polar form is defined by radial window $W(r)$ and angular windows $V(t)$, satisfying the admissibility conditions as

$$\sum_{j=-\infty}^{\infty} W^2(2^j r) = 1 \ , r \in (\frac{3}{4}, \frac{3}{2}) \quad (7)$$

$$\sum_{l=-\infty}^{\infty} V^2(t-l) = 1 \ , t \in (-\frac{1}{2}, \frac{1}{2}) \quad (8)$$

In the frequency domain, $U_j \forall j \geq j_0$ the frequency window is defined as,

$$U_j(r,\theta) = 2^{-3j/4W\left(2^j r\right)V\left(\frac{2^{j/2}\theta}{2\pi}\right)} \quad (9)$$

where $\lfloor j/2 \rfloor$ is the integer part of $j/2$. Thus the support of U_j is a polar wedge defined by support of W and V and is applied with scale dependent windows, with widths in radial and angular direction.

The curvelet are defined as function of $x = (x_1, x_2)$ defined at scale $2^{(-j)}$ angular orientation θ_l and position $x_k^{(j,l)} = R_{\theta_l}^{-1}(k_1 2^{-j}, k_2 2^{-j/2})$ by $\varphi_{j,l,k}(x) = \varphi_j(R_{\theta_l}\left(x - x_k^{(j,l)}\right))$ where, $R_\theta = \begin{pmatrix} \cos\theta & \sin\theta \\ -\sin\theta & \cos\theta \end{pmatrix}$, ${R_\theta}^{-1} = {R_\theta}^{\mathrm{T}} = R_{-\theta}$. A curvelet coefficient in the inner product between an element $f(x) \in L^2(R^2)$ and a curvelet $\varphi_{j,k,l}$.

$$c(j,k,l) = \int_{R^2} f(x)\varphi_{j,k,l}(x)dx \quad (10)$$

where R denotes real line. The curvelet transform can be implemented in two ways ,one using the unequispaced Fast Fourier transform (FFT) and secondly using the wrapping technique [19]. In the current curvelet transform via wrapping has been used.

3 Experimental Work

3.1 Dataset

In the current study the mammogram images were obtained from the Mammographic Image Analysis Society (MIAS) [20] data set and the Image Retrieval in Medical Applications (IRMA) [21] dataset. The MIAS are UK based research groups that work on breast cancer and have generated the digital mammograms dataset for their research. The screening mammograms were

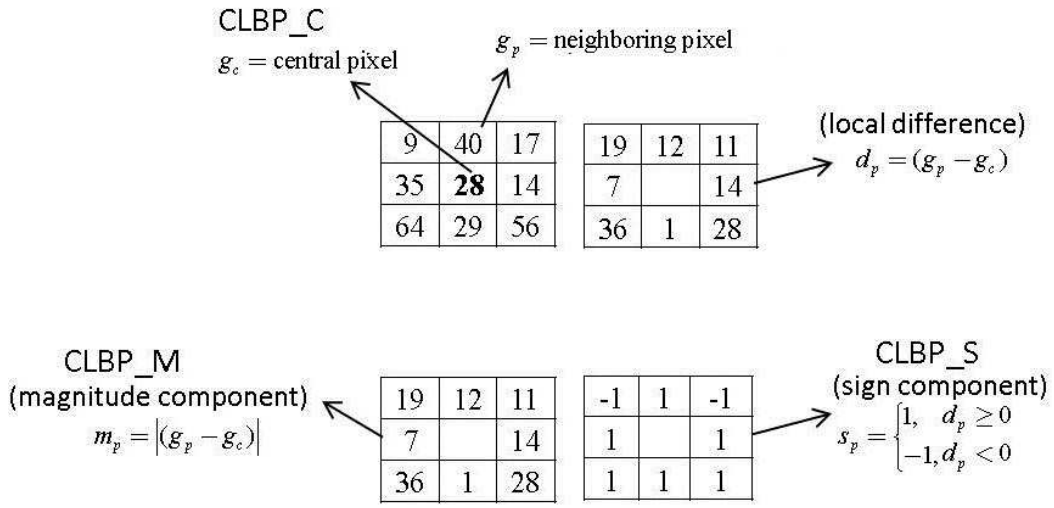

Fig. 1: (a) 3x3 neighborhood block size (b) the local difference d_p(c) m_p the magnitude; and (d) the sign s_p.

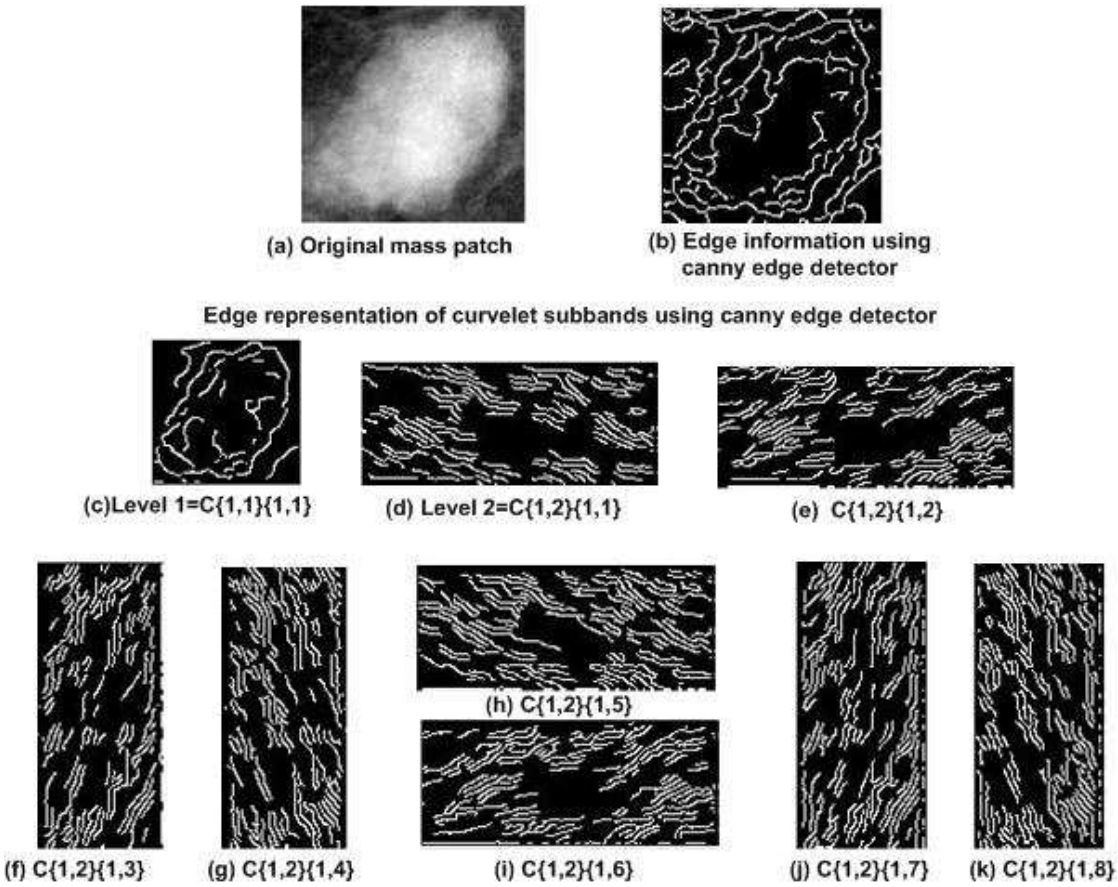

Fig. 2: (a) original mass patch (b) edge information of original image using canny,(c) edge information at level 1,(d-k) edge representations for level 2 at 8 different angles of the curvelet subbands is presented using canny detector.

digitized to 50 micron pixel edge. The MIAS data set contains total of 322 mammogram images. The dataset provides the details, about the location and radii of the abnormalities marked by expert radiologists. In the MIAS dataset the mammogram originally were of 1024×1024 pixels [21]. The preprocessing step was applied to limit the search for abnormalities by removing the background and selecting the region of interest (ROI) before any classification process could be applied on the mammograms.

In the preprocessing step, the background noise, image annotations and the pectoral muscles were removed. Then ROIs of 128×128 were cropped from the processed abnormal mammograms. These ROIs were extracted based on the information provided by the radiologists in the MIAS dataset. Similarly the normal mammograms 128×128 were also cropped manually from the MIAS dataset. In the next step, only mass patches depending on the size of the mass were extracted from the ROIs. The position of patch selection in the abnormal mammogram was based on the information about mass centers provided in the data set. As the mass patches were varying in size, for the normal mammogram we also selected different patches from different locations with varying sizes.

IRMA is a collaborative project between Department of radiology, medical informatics, computer science and Medical Image Processing department at Aachen University. The IRMA dataset is a collection of different dataset like Digital Database for Screening Mammography (DDSM), Lawrence Livermore National Laboratory (LLNL) and Rheinisch-Westf alische Technische Hochschule (RWTH)database and contains more than $30,000$ mammogram images with available ground truths by radiologists [21]. The current study utilizes the non-commercial class that contains different texture patterns of 128×128 pixels each extracted from the mammogram of different BIRADS by expert radiologists.

In the Experimental work, a total of 513 patches obtained from IRMA and MIAS datasets were used. There were 224 cases of Normal cases 289 cases of masses taken from MIAS and IRMA .The abnormal class includes masses, circumscribed masses, ill-defined masses, spiculated masses and architectural distortion (Table 1).

From the literature it was noted that most of the mass size detected in clinical screening programmes lies within 5mm to 32 mm [22]. Thus keeping in view the size of masses minimum criteria was set to extract patches from the ROIs i.e. window size should not be less than 20×20 pixels for extracting the mass patches from the abnormal ROIs.

Table 1: The distribution of selected cases from the MIAS and IRMA dataset

Class	MIAS dataset	IRMA dataset	Total
Circumscribed masses	23	97	120
Masses	–	82	82
Ill-defined masses	14	–	14
Spiculated masses	19	27	46
Architectural distortions	19	8	27
Normal tissue	142	82	224
Total			513

3.2 Feature Extraction

This work aims to improve the classification accuracy for normal and abnormal mammograms by reducing the false positive (FP) alarms. Thus we propose fusion of texture features obtained from two state of the art methods. The features from the ROI patches are extracted using local binary pattern and its extension the completed local binary patterns and curvelet transform.

First, we compute CLBP features using three different values of (P,R) using the uniform rotationally invariant mapping. For each LBP (i.e. CLBP_S), CLBP_M, CLBP_M/C ,CLBP_S_M/C, CLBP_S/M, CLBP_S/M/C we compute texture features using (P=8, R=1), (P=16, R=2), (P=24, R=3). The number of features varies with varying neighborhood and radius value for each of transitions of CLBP. Secondly following the footprints of our previous work [6], we apply curvelet via warping transform and compute grey level texture features from the curvelet sub-band coefficients.

In the current study two levels of sub-band decomposition are used because of the size of ROI patches. The two level sub-band produced 9 matrices (one matrix for level 1 and 8 matrices for level 2, Figure 2) with varying size that yield 9 grey level texture matrices. For each matrix nine features are computed that include energy, contrast, homogeneity, correlation, entropy, mean, standard deviation, moment and maximum probability. From two levels of curvelet decomposition, a curvelet features matrix of size 513×81 is obtained, while feature matrix for CLBP transitions varies with varying values of P, R (see Table 2). Evaluation of feature matrices obtained by both methods, separately done using the nearest neighbor classifier and the performance metrics for each method are recorded.

In the final step texture features from CLBP and curvelet are combined together to obtain the feature fusion matrix. Then the fused feature matrix is passed to classifier.

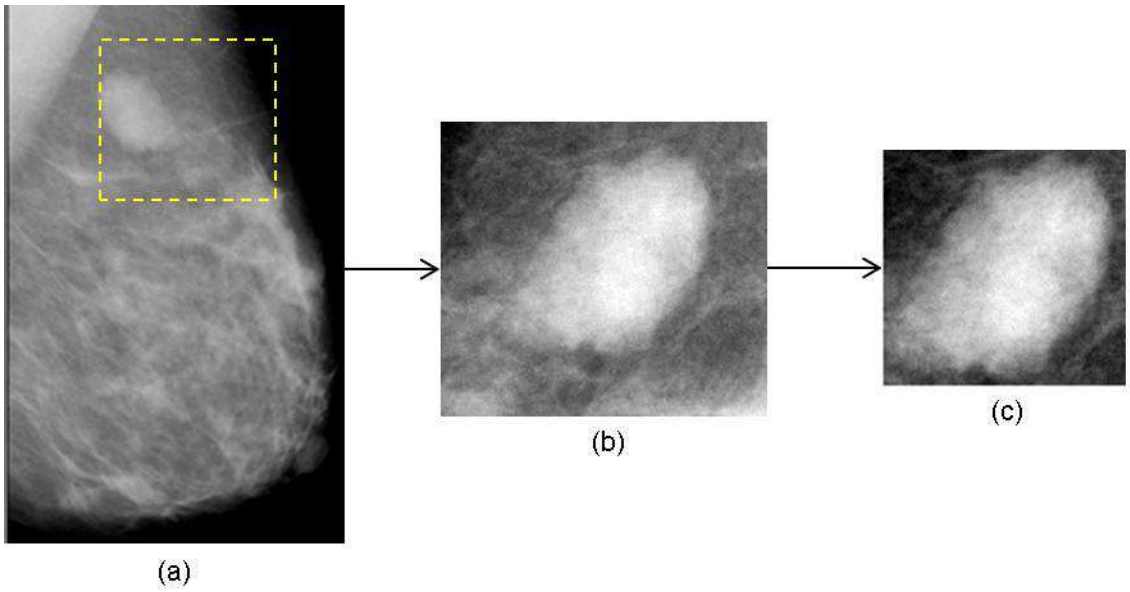

Fig. 3: Extracting the mass patch from MIAS dataset (a) original mammogram 1024×1024, (b) ROI cropped 128×128, (c) Mass patch extracted from the ROI.

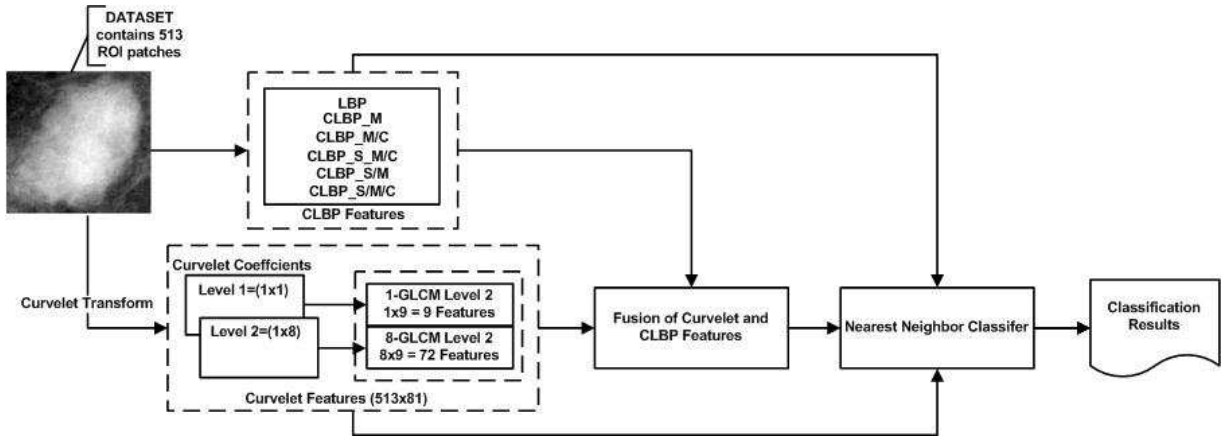

Fig. 4: Frame work for Fusion.

3.3 Classification and performance evaluation

Nearest Neighbor (NN) classifier is used for classification of masses and normal patches using 10 fold cross validation. The performance of the system is evaluated using 1 nearest neighbor (1NN) firstly on the features obtained from local binary pattern and its variants the secondly the classification task for curvelet sub-band matrices are performed. In the last step the 1NN evaluates the performances on the combined features matrices obtained after fusion of curvelet and LBP and its variants features.

In this work, a method to extract texture features by fusion of Curvelet and CLBP techniques is investigated that is expected to improve classification accuracy by false positive reduction in mammograms. Performance of developed method is evaluated by calculating metrics such as Accuracy, Sensitivity and Specificity [23,24] as expressed in Equations (11), (12) and (13) respectively.

$$accuracy = \frac{TPs + TNs}{TPs + TNs + FPs + FNs} \tag{11}$$

$$sensitivity = \frac{TPs}{TPs + FNs} \tag{12}$$

$$specificity = \frac{TNs}{TNs + FPs} \tag{13}$$

4 Statistical Analysis

Once the performance is measured using the equations given above, a test to measure significance of obtained results was conducted using t-test as it provides an estimate for the acceptance and rejection of the significance level among multiple methods used [25] for the significance of the technique developed, t-test is performed between the methods that use fusion and without fusion using Equation (14)

$$t = \frac{\bar{x} - \bar{y}}{\sqrt{\frac{s_x^2}{n} + \frac{s_y^2}{m}}} \tag{14}$$

where $\bar{x}$ and $\bar{y}$ are the means and s_x, s_y are the standard deviations of sample x and y with $(n+m-2)$ degrees of freedom.

5 Results and Discussion

The evaluation of the system was carried in two steps. In the first step, the feature vectors from CLBP and Curvelet were classified separately to evaluate the performance individually with respect to accuracy, sensitivity and specificity. In the second step, fusion of features obtained from CLBP and Curvelet is performed followed by the classification using 1NN. Performance of CLBP with various transitions along with different neighborhoods (P) and radius (R) as well as features extracted using Curvelet are tabulated in Table (2).

Table (2) shows that the performance metrics of features extracted using curvelet and variants of CLBP. As shown in Table (2), with an increase in the size of neighborhood as well as radius, numbers of extracted features are increasing that show improved performance of CBBP method and its variants. The system performance has achieved maximum accuracy of 94.7% classification when CLBP_S is concatenated with joint histogram of CLBP_M/C i.e. CLBP_S_M/C. Increased performance at P=24 and R=3 is obvious compared to results obtained at P=8, 16 and R=1, 2 due to the fact that computation of local texture information is performed in depth at more number of neighborhood.

However, it has also been found that with an increase in number of extracted features obtained using increased value of P and R, performance of the method results in slightly lower accuracy and sensitivity, particularly in the case of CLBP_S/M/C. That might be due to redundancy of features extracted.

Besides the CLBP method that has achieved significant accuracy and sensitivity values, accuracy and specificity analysis is also performed for features extracted using curvelet method. An accuracy of 95.51% and sensitivity of 98.2% is achieved using curvelet method that shows significantly better performance than CLBP techniques. This is mainly due to the utilization of

Table 2: Performance of CLBP and Curvelet techniques for different combinations of P and R parameters. The rows entries correspond to Number of features (Fets), accuracy (Acc), Sensitivity (Sen) and Specificity (Spec)

	CLPB_S (LBP)			**CLBP_M**			**CLBP_M/C**			**CLBP_S_M/C**			**CLBP_S/M**			**CLBP_S/M/C**			**Curvelet Features**
	P=8 R=1	P=16 R=2	P=24 R=3	P=8 R=1	P=16 R=2	P=24 R=3	P=8 R=1	P=16 R=2	P=24 R=3	P=8 R=1	P=16 R=2	P=24 R=3	P=8 R=1	P=16 R=2	P=24 R=3	P=8 R=1	P=16 R=2	P=24 R=3	
Fets.	10	18	26	10	18	26	20	34	52	30	54	78	100	324	676	200	648	1352	**81**
Acc.	91.4	93.2	93.4	92.8	92.2	93.4	93.4	92.8	94.2	93.6	94.0	94.7	92.6	92.4	92.8	93.0	93.4	93.0	**95.5**
Sen.	93.1	92.7	92.7	94.1	92.4	93.1	92.4	92.4	92.7	93.8	94.1	92.7	92.4	90.3	90.7	92.0	91.7	90.0	**98.2**
Spec.	89.3	93.8	94.2	91.1	92.0	93.8	94.6	93.3	96.0	93.3	93.8	97.3	92.9	95.1	95.5	94.2	95.5	96.9	**92.4**

scaling law that results in superior direction and sparse representation of edges during the implementation of curvelet to reconstruct an image as depicted in Figure (2) of Section (2.3) in this paper. Furthermore, the false positive rates for curvelet is presented in the given confusion matrix.

Confusion matrix for Curvelet

a	**b ← classified as**
271	**18** | **a = mass**
5	**219** | **b = normal**

As discussed in the Introduction section of this paper, the main objective is to perform fusion of CLBP features with curvelet features for false positive reduction to evaluate performance of the system in classifying normal and abnormal ROI patches. To do so, 81 features obtained from curvelet techniques are fused with features obtained using the variants of CLBP techniques. In order to fuse, features obtained from both methods are concatenated that results in fused feature matrix. Furthermore, once the features are fused, classification is performed followed by the evaluation of classifier performance using performance metrics used earlier. Table (3) illustrates the performance of the fusion of features.

As shown in Table (3), addition of curvelet features with variants of CLBP resulted in improved classification rates in all cases except for CLBP_S/M/C_CFET (P=24, R=3) due to the redundant features. It has been found that the method CLBP_S_CFET (CLBP_S combined with curvelet) having 99 features, the system achieves maximum accuracy of 96.7% and sensitivity of 98.9% with (P=16, R=2) as compared to other variants of CLBP. From the analysis, it is found that fusion of curvelet with CLBP_S provides the most accurate classification.

Furthermore, the false positive rates of selected fused method as compared to variants of CLBP and curvelet are also measured and the values are reported in Figure 5.

Table 3: Performance of fusion matrix obtained from different combination of P and R parameters. The rows entries correspond to Number of features (Fets), accuracy (Acc), Sensitivity (Sen) and Specificity (Spec)

	CLPB_S (LBP)_CFET			**CLBP_M_CFET**			**CLBP_M/C_CFET**			**CLBP_S_M/C_CFET**			**CLBP_S/M_CFET**			**CLBP_S/M/C_CFET**		
	P=8 R=1	P=16 R=2	P=24 R=3	P=8 R=1	P=16 R=2	P=24 R=3	P=8 R=1	P=16 R=2	P=24 R=3	P=8 R=1	P=16 R=2	P=24 R=3	P=8 R=1	P=16 R=2	P=24 R=3	P=8 R=1	P=16 R=2	P=24 R=3
Fets.	91	99	107	91	99	107	101	99	133	111	99	159	181	405	757	281	729	1433
Acc.	96.3	96.7	96.2	96.5	96.3	96.1	96.1	96.3	96.1	95.7	95.7	95.7	95.7	95.1	93.9	94.9	94.5	91.2
Sen.	99.2	98.9	99.3	99.2	98.6	98.9	98.9	98.6	98.2	97.9	98.2	97.5	98.6	97.8	94.8	97.8	97.8	94.2
Spec.	92.8	94.1	92.8	93.2	93.6	92.8	92.7	93.6	93.5	93.1	92.7	93.5	92.4	91.9	92.8	91.5	90.5	87.7

Table 4: The results of t-test at $\alpha = 0.1\%$ for enhanced CLBP against CLBP methods

Method	**P-value**	**Null hypothesis**
CLBP_S_CFET vs CLBP_S	0.0047	Reject
CLBP_M_CFET vs CLBP_M	6.6204×10^{-4}	Reject
CLBP_M/C_CFET vs CLBP_M/C	0.0028	Reject
CLBP_S_M/C_CFET vs CLBP_S_M/C	0.0076	Reject
CLBP_S/M_CFET vs CLBP_S/M	0.0132	Reject
CLBP_S/M/C_CFET vs CLBP_S/M/C	0.7517	Accept

As seen from Figure (5), number of false positive (FP) obtained from curvelet technique are less compared to all CLBP methods. In addition, it is clearly seen that with the addition of curvelet features to the CLBP texture features, significantly contributes in reducing false positive (FP)

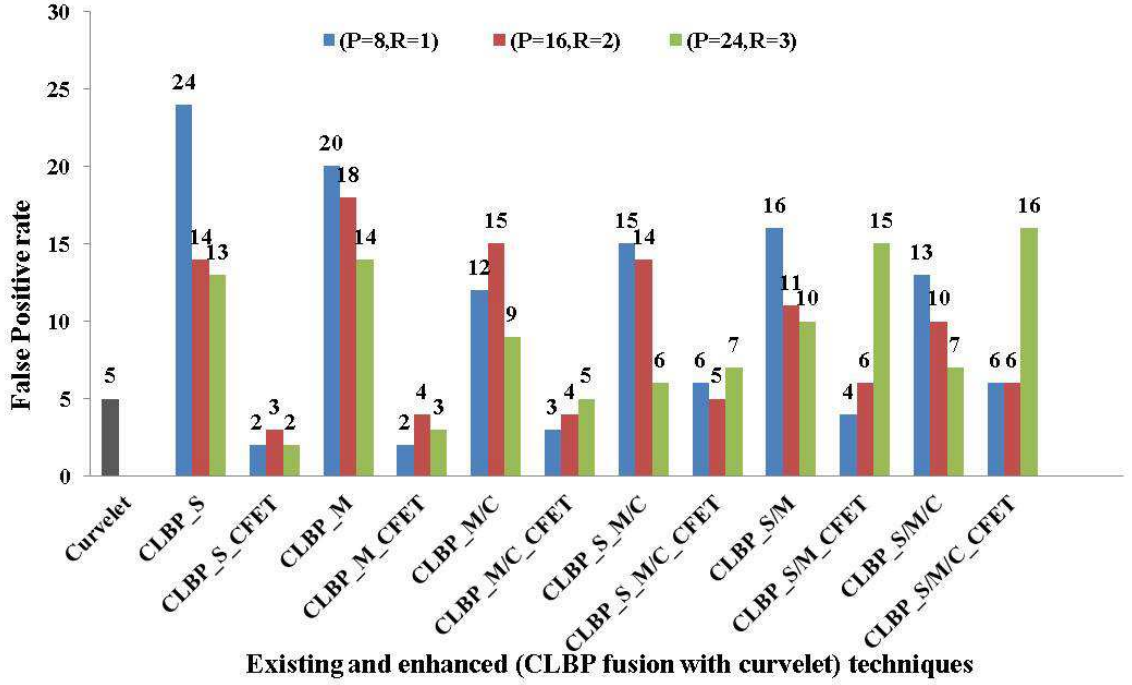

Fig. 5: Existing and enhanced (CLBP fusion with curvelet) techniques for false positive reduction.

rates and even produces less FPs as compared to curvelet itself. Moreover, the enhanced techniques the classification accuracies and sensitivities are significantly improved in all cases except for (P = 24, R=3) in CLBP_S/M/C_CFET where the accuracy reduced from 93% to 91% (Table 2 and Table 3). Comparing the best chosen CLBP_S_CFET (16, 2) with the curvelet confusion matrix and CLBP_S (16, 2) we notice that FP rate is reduced by 40% and 78% respectively (Figure 5).

Table 5: The results of t-test at $\alpha = 0.1\%$ best chosen CLBP vs other enhanced CLBP methods

Method	**P-value**	**Null hypothesis**
CLBP_S_CFET vs CLBP_M_CFET	0.6291	Accept
CLBP_S_CFET vs CLBP_M/C_CFET	0.2341	Accept
CLBP_S_CFET vs CLBP_S_M/C_CFET	0.0102	Reject
CLBP_S_CFET vs CLBP_S/M_CFET	0.0528	Reject
CLBP_S_CFET vs CLBP_S/M/C_CFET	0.0724	Reject

Since the classifier has shown a good performance with less FP rates, it is if further tested to investigate the clinical significance. A hypothesis testing is performed to check the difference in performance of CLBP techniques versus the CLBP combined with curvelet features where a t-test for significance level $\alpha = 0.1\%$ was used. For this, null hypothesis was rejected with $p - values < 0.1$. Similarly, the significance of best chosen CLBP_S_CFET was tested against all CLBP techniques fused with curvelet at $\alpha = 0.1\%$. Results obtained from the t-tests are shown in Table (4) and Table 5 for p-values obtained.

P-values obtained from the t-test enhanced CLBP obtained from fusion and variants of CLBP methods are reported in Table (4). The null hypothesis are rejected for all the cases where p-values are very small (< 0.1) that represents the significance of the test. It is also found that t-test performed on CLBP_S/M/C_CFET and CLBP_S/M/C method is insignificant and null hypothesis cannot be rejected due to the large p-values (> 0.1) as tabulated in Table (4).

Similarly, the significance of best chosen (CLBP_S_CFET) method compared to other enhanced CLBP methods are tabulated in Table (5). From Table (5), it can be observed that last three methods are significant as they represents $p - values < 0.1$. Although, the techniques such as CLBP_M_CFET and CLBP_M/C_CFET are significant as compared to variants of CLBP as discussed in Table (4) but resulting in insignificant values against best chosen method (CLBP_S_CFET) where the null hypothesis is not rejected. This is mainly due to the small variation in accuracies (± 0.16) of CLBP_M_CFET and

Table 6: Comparison with existing methods

Method	Data Set	Classifier	Accuracy (%)	Area under Curve (AUC) value
Oliver et.al. [7] presented mammogram classification by using LBP and co-occurrence matrices features.	The MIAS dataset 322 mammograms was used the segmentation task was performed using the Fuzzy C-Means algorithm ,normalized cut and the Mean Shift algorithms .	The classification performance of features obtained from each segmentation was tested using KNN, linear discriminant analysis, binary tree and Support vector machine.	KNN with leave one out (LOO) produced the maximum accuracy of 0.78	
Oliver et.al. [8] presented a method to reduce False positive rates using the local binary patterns.	The experiments were performed using DDSM data set with 1792 suspicious regions containing 1536 normal and 256 mass samples	Support Vector Machines (SVM).	0.9060 ± 0.043.	
Paquerault et.al [9] fused textural features and morphological features	The data used contains 169 pairs of cranio-caudal (CC) and mediolateral oblique (MLO) view of the mammograms collected at University of Michigan (UM).	Linear discriminant analysis was used for classification.	The system showed maximum accuracy of 91%	
Duarte et.al. [10] used completed local binary pattern (CLBP) and wavelet transform for feature extraction to classify the mammogram lesions.	The dataset used in the study contains 720 mammogram from DDSM database with 240 normal, 240 benign lesion and 240 malignant lesion samples.	Most significant features are selected by performing ANOVA. Later on SVM classifier was used for classification		The multiresolution produced AUC value 0f 1.0 as compared to CLBP with AUC value 0.89
Gardezi et.al. [6] combined the GLCM texture feature from curvelet with features obtained directly form mammogram images	305 MIAS mammogram images were used to get region of interest (ROIs with 207 normal (ROIs) and 98 mass (ROIs).	The simple logistic classifier was used for the classification task.	0.886	AUC value of 0.91
Choi et.al [12] extracted multiresolution LBP features from the mammogram ROIs that have ability to characterize the regional texture patterns and margin regions of a mass.	MIAS and DDSM dataset were used in the study. A total of 391 mammograms were investigated 89 MIAS (72 mass ROIs and 1 621 normal tissue ROIs) and 303 DDSM mammogram images (246 mass ROIs and 2 497 normal tissue ROIs).	The classification task was performed using the SVM-RFE (recursive Feature elimination) classifier	Method achieves 0.9631 and 0.8741 accuracies for MIAS DDSM dataset respectively.	
Hussain [13] extracted the texture features using the multiscale spatial WLD (MSWLD) method to classify the mass and normal class tissues.	1024 ROIs from DDSM dataset were selected	SVM classifier has been used for classification		AUC Value of 0.99 $\pm$ 0.003.
The Proposed Fusion method	513 mammogram ROI patches containing contains 224 normal and 289 abnormal mammogram ROI patches, extracted from MIAS and IRMA datasets.	1NN classifier is used	96.7 $\pm$ 0.16 classification accuracy with 98.9% sensitivity.	

CLBP_M/C_CFET with best chosen CLBP_S_CFET method as mentioned in Table (3).

The proposed method was evaluated against existing methods that use the fusion of features to classify the normal and abnormal tissues in mammogram images. The comparison of the performance metrics of our proposed method and the existing methods is shown in table (6).

From the comparison above, it can be seen that performance of the proposed method is comparable with the existing techniques and even better in some of the cases listed above. In summary, the significant contribution of current study can be confirmed from the results obtained in this research, that enhancement of CLBP technique by fusion of curvelet features not only led to an improvement in accuracy and sensitivity (reduction in false positive rate) of classifier but also provide statistically significant outcomes that are potentially applicable for clinical practices. However, the proposed method has some limitation; it is dependent on the size of the ROI patches.

6 Conclusion

In this paper a method to reduce the false positives is presented by fusion of texture features. Firstly individual performances of features obtained CLBP methods with varying neighborhoods(P) and radius(R) and features obtained from curvelet are measured using the performance metrics i.e. accuracy, sensitivity and specificity using the INN classifier. The false positive (FP) produced by each method were also recorded. The experimental results show that curvelet produced better results with an accuracy of 95.51% as compared to 94.7%. The better performance of curvelet is due to its directional feature and good edge representation (Figure 2). In the later stage, feature fusion was carried by combining the features of CLBP variants and curvelet sub-band features to obtain enhanced CLBP variants. The classification results show an overall improvement of classification accuracy as well as sensitivity in all enhanced CLBP techniques as compared to CLBP variants and the results are statistically significant. The false positive rates are reduced significantly for all enhanced CLBP methods in comparison to curvelet and CLBP variants. Amongst the enhanced CLBP methods, CLBP_S_CFET produces the best classification accuracy of 96.68% with sensitivity of 98.9%. The results have shown that fusion of texture features are effective and have efficiently reduced the false positive rates in mammogram classification. In future work, we plan to investigate the performance of the proposed feature extraction method by increasing the ROI sizes with and without application of some filtering technique.

Acknowledgment

The work is supported by URIF grant 0153AA-B52.

References

[1] ”Latest world cancer statistics Global cancer burden rises to 14.1 million new cases in 2012:Marked increase in breast cancers must be addressed,” ed. Lyon/Geneva: International Agency for Cancer Research (IARC) ,World Health Organisation (WHO), 2013.

[2] M. Mirmehdi, X. Xie, and J. Suri, Handbook of Texture Analysis: Imperial College Press, 2009.

[3] M. M. Eltoukhy, I. Faye, and B. B. Samir, ”A statistical based feature extraction method for breast cancer diagnosis in digital mammogram using multiresolution representation,” Comput. Biol. Med., **42**, 123-128, (2012).

[4] I. Christoyianni, A. Koutras, E. Dermatas, and G. Kokkinakis, ”Computer aided diagnosis of breast cancer in digitized mammograms,” Computerized Medical Imaging and Graphics, **26**, 309-319, (2002).

[5] A. Karahaliou, S. Skiadopoulos, I. Boniatis, P. Sakellaropoulos, E. Likaki, G. Panayiotakis, et al., ”Texture analysis of tissue surrounding microcalcifications on mammograms for breast cancer diagnosis,” The British Journal of Radiology, **80**, 648-656, (2007).

[6] S. J. S. Gardezi, I. Faye, and M. M. Eltoukhy, ”Analysis of mammogram images based on texture features of curvelet Sub-bands,” in Fifth International Conference on Graphic and Image Processing, 2014, pp. 906924-906924-6.

[7] A. Oliver, X. Llado, R. Marti, J. Freixenet, and R. Zwiggelaar, ”Classifying mammograms using texture information,” in Medical Image Understanding and Analysis, 2007, pp. 223-227.

[8] A. Oliver, X. Llad, J. Freixenet, and J. Mart, ”False positive reduction in mammographic mass detection using local binary patterns,” in Medical Image Computing and Computer-Assisted Intervention?MICCAI 2007, ed: Springer, 2007, pp. 286-293.

[9] S. Paquerault, N. Petrick, H. P. Chan, B. Sahiner, and M. A. Helvie, ”Improvement of computerized mass detection on mammograms: Fusion of two-view information,” Medical Physics, **29**, 238-247 (2002).

[10] Y. Duarte, M. Nascimento, and D. Oliveira, ”Classification of mammographic lesion based in Completed Local Binary Pattern and using multiresolution representation,” in Journal of Physics: Conference Series, 2014, p. 012127.

[11] M. M. Eltoukhy, I. Faye, and B. B. Samir, ”Curvelet based feature extraction method for breast cancer diagnosis in digital mammogram,” in Intelligent and Advanced Systems (ICIAS), 2010 International Conference on, 2010, pp. 1-5.

[12] J. Y. Choi and Y. M. Ro, ”Multiresolution local binary pattern texture analysis combined with variable selection for application to false-positive reduction in computer-aided detection of breast masses on mammograms,” Physics in medicine and biology, **57**, 7029 (2012).

[13] M. Hussain, ”False-positive reduction in mammography using multiscale spatial Weber law descriptor and support vector machines,” Neural Computing and Applications, **25**, 83-93 (2014).

[14] R. M. Haralick, K. Shanmugam, and I. H. Dinstein, "Textural features for image classification," Systems, Man and Cybernetics, IEEE Transactions on, pp. 610-621, 1973.
[15] S. Arivazhagan and L. Ganesan, "Texture classification using wavelet transform," Pattern recognition letters, **24**, 1513-1521 (2003).
[16] T. Ojala, M. Pietikainen, and T. Maenpaa, "Multiresolution gray-scale and rotation invariant texture classification with local binary patterns," Pattern Analysis and Machine Intelligence, IEEE Transactions on, **24**, 971-987 (2002).
[17] Z. Guo and D. Zhang, "A completed modeling of local binary pattern operator for texture classification," Image Processing, IEEE Transactions on, **19**, 1657-1663 (2010).
[18] E. J. Candes and D. L. Donoho, "Curvelets, multiresolution representation, and scaling laws," 2000, pp. 1-12.
[19] E. Cands, L. Demanet, D. Donoho, and L. Ying, "Fast discrete curvelet transforms," Multiscale Modeling and Simulation, **5**, 861-899 (2006).
[20] S. A. J Suckling, D Betal, N Cerneaz, D R Dance, S-L Kok, J Parker, I Ricketts, J Savage, E Stamatakis and P Taylor, "The Mammographic Image Analysis Society Digital Mammogram Database Exerpta Medica," International Congress Series, **1069**, 375-378 (1994).
[21] J. E. Oliveira, M. O. Gueld, A. d. A. Arajo, B. Ott, and T. M. Deserno, "Toward a standard reference database for computer-aided mammography," in Medical Imaging, 2008, pp. 69151Y-69151Y-9.
[22] J. Michaelson, S. Satija, R. Moore, G. Weber, E. Halpern, A. Garland, et al., "Estimates of the sizes at which breast cancers become detectable on mammographic and clinical grounds," Journal of Womens Imaging, **5**, 3-10 (2003).
[23] R. Parikh, A. Mathai, S. Parikh, G. Chandra Sekhar, and R. Thomas, "Understanding and using sensitivity, specificity and predictive values," Indian Journal of Ophthalmology, **56**, 45-50 (2008).
[24] A. G. Lalkhen and A. McCluskey, "Clinical tests: sensitivity and specificity," Continuing Education in Anaesthesia, Critical Care & Pain, **8**, 221-223 (2008).
[25] T. G. Dietterich, "Approximate statistical tests for comparing supervised classification learning algorithms," Neural computation, **10**, 1895-1923 (1998).

Syed Jamal Safdar Gardezi received his BS and MS in Applied Mathematics from COMSATS Institute of IT Islamabad, Pakistan in 2008 and 2010. He is currently working as PhD scholar in Department of Fundamental and Applied Sciences at University Teknologi PETRONAS since Sept 2012.His research focuses on developing an automatic lesion segmentation algorithm to reduce false positive rates in breast cancer detection.

Ibrahima Faye received a BSc, MSc and PhD in Mathematics from University of Toulouse and a MS in Engineering of Medical and Bio-technological data from EcoleCentrale Paris. He is currently Associate Professor at the Department of Fundamental and Applied Sciences of Universiti Teknologi PETRONAS. His research interests include Engineering Mathematics, Signal & Image Processing, Pattern Recognition, and Dynamical Systems. He is member of IEEE, EMBS and French Mathematical Society.